Submitted to the
32nd International Conference on High Energy Physics
August 16 - 22, 2004, Beijing, China

Abstract: 5-0291 **Session: QCDhard**

Forward jet production in deep inelastic ep scattering and low x parton dynamics at HERA

ZEUS Collaboration

Abstract

Differential inclusive jet cross sections in neutral current deep inelastic *ep* scattering have been measured with the ZEUS detector using an integrated luminosity of 38.7 pb^{-1}. The jets have been identified using the k_T cluster algorithm in the longitudinally invariant inclusive mode in the laboratory frame and selected with jet transverse energy, $E_T^{\rm jet}$, above 6 GeV and jet pseudorapidity, $\eta^{\rm jet}$, between -1 and 3. Measurements of cross sections as functions of $E_T^{\rm jet}$, $\eta^{\rm jet}$, Bjorken x and Q^2, the photon virtuality, are presented. Three phase-space regions have been selected to study parton evolution and to compare to the DGLAP and BFKL pQCD approaches. Leading-logarithm parton-shower Monte Carlo models and next-to-leading-order QCD calculations which incorporate DGLAP evolution do not describe the data. Those models with a BFKL-like evolution give a better description of the data.

1 Introduction

In deep inelastic scattering (DIS) of leptons off protons, the momentum distributions of the partons in the proton are probed. The evolution of the momentum distributions as a function of the virtuality, Q^2, of the exchanged boson is predicted by perturbative QCD (pQCD) via renormalization equations. The evolution equations can be derived by resummations in terms of $\ln Q^2$ (DGLAP [1] evolution) or in terms of $\ln(1/x_{\rm Bj})$, where $x_{\rm Bj}$ is the fraction of the proton momentum carried by the struck parton in quark-parton model (QPM) events (BFKL equation [2]). The CCFM equation [3] interpolates between the BFKL and DGLAP equations by means of angular ordering of parton emissions. The DGLAP equations have been tested extensively at HERA [4–10], and were found to describe the data, in general, very well. However, the BFKL approach is expected, in principle, to describe the data better in the lowest $x_{\rm Bj}$ regions of phase space.

In the DGLAP formalism, the parton cascade that results from the hard scattering of the virtual photon with a parton from the proton is ordered in parton virtuality. This ordering along the parton ladder implies an ordering in transverse energy of the partons, with the parton participating in the hard scatter having the highest transverse energy. In the BFKL formalism, there is no strict ordering in virtuality and transverse energy (see Fig. 1). Since the partons emitted at the bottom of the ladder are closest in rapidity to the outgoing proton, they manifested themselves as forward jets. BFKL evolution predicts that a larger fraction of small $x_{\rm Bj}$ events will contain high E_T forward jets than is predicted by DGLAP [11].

In previous studies [12–14] of forward jets in DIS, data were compared to Monte Carlo simulations which model higher order parton emissions using DGLAP equations. These models do not describe the data. However, when a resolved photon contribution [15] was included, a better description was obtained. The calculations based on the Colour-Dipole Model (CDM) [16], which include parton emissions not ordered in transverse energy, also described the data. In a more recent analysis [9], fixed- order QCD calculations were compared to the data. The predictions fail to describe the measurements in the most forward region at low $E_T^{\rm jet}$ and Q^2.

In this paper, measurements of differential inclusive jet cross sections in deep inelastic scattering are presented in three different phase space regions, from the most global to the most restrictive region, where the contribution of events exhibiting BFKL characteristics should be enhanced. The measurements were done in the laboratory frame, as opposed to previous studies, for better accessibility to low values of $x_{\rm Bj}$ and for increased resolution for identifying jets in the forward region of the detector. The selection of $\mathcal{O}(\alpha_s)$ events was done by cutting on the angle γ_h, which corresponds to the direction of the scattered quark in the quark parton model. The jets were reconstructed using the

k_T cluster algorithm in the longitudinally invariant mode, instead of the cone algorithm used in previous studies [12–14], which allows a reduction of the theoretical uncertainty coming from matching the experimental and theoretical algorithms. Inclusive jet cross sections were measured as functions of $E_T^{\rm jet}$, $\eta^{\rm jet}$, Q^2 and $x_{\rm Bj}$. Fixed order QCD predictions based on DGLAP evolution were compared to the data. The uncertainties of the calculation were investigated to determine the regions of phase space where the DGLAP scheme holds. In addition, leading-logarithm parton-shower Monte Carlo models based on DGLAP evolution and CDM were compared to the data.

2 Experimental set-up

The data sample used in this analysis was collected with the ZEUS detector at HERA and corresponds to an integrated luminosity of 38.7 ± 0.6 pb^{-1}. During 1996-1997, HERA operated with protons of energy $E_p = 820$ GeV and positrons of energy $E_e = 27.5$ GeV. A detailed description of the ZEUS detector can be found elsewhere [17, 18]. A brief outline of the components that are most relevant for this analysis is given below. Charged particles are tracked in the central tracking detector (CTD) [19], which operates in a magnetic field of 1.43 T provided by a thin superconducting solenoid. The CTD consists of 72 cylindrical drift-chamber layers, organized in nine superlayers covering the polar-angle [1] region $15° < \theta < 164°$. The transverse-momentum resolution for full-length tracks can be parameterised as $\sigma(p_T)/p_T = 0.0058 p_T \oplus 0.0065 \oplus 0.0014/p_T$, with p_T in GeV. The tracking system was used to measure the interaction vertex with a typical resolution along (transverse to) the beam direction of 0.4 (0.1) cm and to cross-check the energy scale of the calorimeter.

The high-resolution uranium–scintillator calorimeter (CAL) [20] covers 99.7% of the total solid angle and consists of three parts: the forward (FCAL), the barrel (BCAL) and the rear (RCAL) calorimeters. Each part is subdivided transversely into towers and longitudinally into one electromagnetic section (EMC) and either one (in RCAL) or two (in BCAL and FCAL) hadronic sections (HAC). The smallest subdivision of the calorimeter is called a cell. Under test-beam conditions, the CAL single-particle relative energy resolutions were $\sigma(E)/E = 0.18/\sqrt{E}$ for electrons and $\sigma(E)/E = 0.35/\sqrt{E}$ for hadrons, with E in GeV.

[1] The ZEUS coordinate system is a right-handed Cartesian system, with the Z axis pointing in the proton beam direction, referred to as the "forward direction", and the X axis pointing left towards the centre of HERA. The coordinate origin is at the nominal interaction point. The pseudorapidity is defined as $\eta = -\ln(\tan\frac{\theta}{2})$, where the polar angle, θ, is measured with respect to the proton beam direction.

The luminosity was measured from the rate of the bremsstrahlung process $ep \rightarrow e\gamma p$. The resulting small-angle energetic photons were measured by the luminosity monitor [21], a lead-scintillator calorimeter placed in the HERA tunnel at $Z = -107$ m.

3 Definition of the cross sections

Jet production in NC DIS up to LO in α_s proceeds as in the QPM ($Vq \rightarrow q$, where $V = \gamma$ or Z^0) or via the boson-gluon fusion (BGF, $Vg \rightarrow q\bar{q}$) and QCD-Compton (QCDC, $Vq \rightarrow qg$) processes. Measurements of inclusive jet cross sections were made in three different phase-space regions. Jets were identified using the k_T cluster algorithm [22] in the longitudinally invariant inclusive mode [23] in the laboratory frame. The first region, called "global", was designed to be as inclusive as possible to keep the theoretical uncertainties small. This region was defined by the conditions:

- $Q^2 > 25$ GeV^2;
- $y > 0.04$, where y is the inelasticity variable;
- $E'_e > 10$ GeV, where E'_e is the energy of the scattered positron;
- and jets with $E_T^{\rm jet} > 6$ GeV and $-1 < \eta^{\rm jet} < 3$ were selected.

This phase-space region is dominated by QPM events.

To isolate the region of phase space where BFKL effects are expected to be larger, a second phase-space region, called "BFKL", was defined by requiring the following additional conditions:

- $\cos\gamma_h < 0$, where γ_h is an angle that corresponds, in the QPM, to the direction of the scattered quark;
- $0 < \eta^{\rm jet} < 3$;
- and $0.5 < \frac{(E_T^{\rm jet})^2}{Q^2} < 2$.

The requirements on γ_h and $\eta^{\rm jet}$ suppress the contribution from QPM events. The requirement on $\frac{(E_T^{\rm jet})^2}{Q^2}$ limits the Q^2 evolution of the particles on the parton ladder.

A third phase-space region, called "forward BFKL", was selected to investigate events with a very forward-going jet and defined by requiring in addition $2 < \eta^{\rm jet} < 3$.

4 Data selection and jet identification

A three-level trigger was used to select events online [18]. The NC DIS events were selected offline using criteria similar to those reported previously [24]. The main steps are outlined below.

The scattered-positron candidate was identified from the pattern of energy deposits in the CAL. The E'_e and polar angle (θ_e) of the positron candidate were also determined from the CAL measurements, after correction for energy loss in inactive material in front of the CAL. The following requirements were imposed on the data sample:

- a positron candidate of energy $E'_e > 10$ GeV. This cut ensured a high and well understood positron-finding efficiency and suppressed background from photoproduction, in which the scattered positron escapes in the rear beampipe;
- the vertex position $|Z_{vtx}| < 50$ cm along the beam axis, determined from CTD tracks;
- $38 < (E - p_z) < 65$ GeV, where E is the total energy measured in the CAL, $E = \sum_i E_i$, and p_Z is the Z component of the vector $\boldsymbol{p} = \sum_i E_i \boldsymbol{r_i}$; in both cases the sum runs over all CAL cells, E_i is the energy of the CAL cell i and $\boldsymbol{r_i}$ is a unit vector along the line joining the reconstructed vertex to the geometric centre of the cell i. This cut removed events with large initial-state radiation and further reduced the background from photoproduction events;
- $y_e < 0.95$, where $y_e = 1 - E'_e(1 - cos\theta_e)/(2E_e)$. This condition removed events in which fake positron candidates from photoproduction background were found in the FCAL;
- $y_{JB} > 0.04$, where $y_{JB} = \sum_i E_i(1 - \cos\theta_i)/(2E_e)$ calculated according to the Jacquet-Blondel method [25], where the sum runs over all CAL cells except those belonging to the scattered positron. The y_{JB} variables is an estimator of y which gives a good resolution at low y;
- $p_T^{CAL}/\sqrt{E_T^{CAL}} < 3\ \sqrt{\text{GeV}}$ where p_T^{CAL} is the total transverse momentum as measured with the CAL and E_T^{CAL} is the total transverse energy in the CAL. This cut removed cosmic rays and beam-related background;
- $|X| > 14$ cm or $|Y| > 14$ cm, where X and Y are the impact positions of the positron on the CAL, to avoid the low-acceptance region adjacent to the rear beampipe;
- the energy not associated with the positron candidate within a cone of radius 0.7 units in $\eta - \phi$ plane around the positron direction was required to be less than 10% of the positron energy. This condition removed photoproduction and DIS events in which a part of a jet was incorrectly identified as the scattered positron.

The kinematic variables Q^2 and x_{Bj} were reconstructed using a combination of the electron and double-angle (DA) methods [26], depending on which method gave a better resolution of the observed scattered positron energy. The angle γ_h was reconstructed with the CAL using:

$$\cos\gamma_h = \frac{\sum_i p_{X,i}^2 + \sum_i p_{Y,i}^2 - \sum_i (E - p_Z)_i^2}{\sum_i p_{X,i}^2 + \sum_i p_{Y,i}^2 + \sum_i (E - p_Z)_i^2} \tag{1}$$

where the sum runs over all CAL cells, excluding those associated with the scattered positron.

The k_T cluster algorithm was used in the longitudinally invariant inclusive mode to reconstruct jets in the hadronic final state from the energy deposits in the CAL cells. The jet algorithm was applied after excluding those cells associated with the scattered-positron candidate. The jet search was performed in the $\eta - \phi$ space in the laboratory frame. The jet variables were defined according to the Snowmass convention [27]. Jet transverse energies were corrected for all energy-loss effects, principally in inactive material, typically about one radiation length, in front of the CAL. After these corrections to the jet transverse energy, events with at least one jet satisfying $E_T^{\rm jet} > 6$GeV and $-1 < \eta^{\rm jet} < 3$ were included in the global data sample. The BFKL and forward-BFKL subsamples were selected using the requirements listed in Sec. 3.

5 Monte Carlo simulation

Samples of events were generated to determine the response of the detector to jets of hadrons and to determine the correction factors necessary to obtain the hadron-level jet cross sections. The generated events were passed through the GEANT 3.13-based [28] ZEUS detector- and trigger-simulation programs [18]. They were reconstructed and analysed by the same program chain as the data.

Neutral current DIS events were generated using the LEPTO 6.5.1 program [29] interfaced to HERACLES 4.6.1 [30] via DJANGOH 1.1 [31]. The HERACLES program includes photon and Z exchanges and first-order electroweak radiative corrections. The QCD cascade was modelled with the CDM as implemented in the ARIADNE 4.08 program [32]; ARIADNE simulates the BGF process in addition. The CDM treats gluons emitted from quark-antiquark (diquark) pairs as radiation from a colour dipole between two partons. This results in partons that are not ordered in their transverse momenta. Samples of events were also generated using the model of LEPTO based on first-order QCD matrix elements plus parton showers (MEPS). For the generation of the samples with MEPS, the option for soft-colour interactions was switched off [33]. In both cases, fragmentation into hadrons was performed using the Lund string model [34] as implemented in JETSET 7.4 [35]. The CTEQ4M [36] proton parton density functions (PDFs) were used for all simulations.

The jet identification was performed using the energy measured in the CAL cells in the same way as for the data. The same jet algorithm was also applied to the final-state particles and to the partons available after the parton shower; the jets found in this way are referred to as hadronic and partonic jets, respectively.

Electroweak-radiative and hadronisation effects are not at present included in the fixed-order QCD programs described below (Sec. 7). The electroweak-radiative effects were determined to be small ($< 5\%$) and corrections for those effects were not included. Samples of MC events were generated to correct the QCD calculations for hadronisation effects. Since the measurements refer to jets of hadrons, whereas the QCD calculations refer to partons, the predictions were corrected to the hadron level using these MC samples. A multiplicative correction factor, δ_{had}, was defined as the ratio of cross sections for jets of hadrons over that for jets of partons, and was computed with the MC programs. The factor applied to the predictions was the average of the correction factors obtained with Ariadne and Lepto. The uncertainty on the hadronization correction was taken to be the absolute difference in the correction factors obtained with Lepto and Ariadne.

6 Measurement of the cross sections

Differential inclusive jet cross sections were measured using the selected data samples, and were corrected for detector acceptance. The Ariadne MC samples of events were used to compute the acceptance corrections. These correction factors took into account the efficiency of the trigger, the selection criteria, and the purity and efficiency of the jet identification, and were generally between 0.8 and 1.2. The inclusive cross sections for jets of hadrons were determined by applying bin-by-bin corrections to the measured distributions. For this approach to be valid, the distributions in the data must be well described by the MC simulations at the detector level. This condition was in general satisfied by both Ariadne and Lepto. The samples of Lepto were used to compute the systematic uncertainties coming from the parton-shower models.

A study of the main sources contributing to the systematic uncertainties of the measurements was performed. These sources were:

- the effect of the treatment of the parton shower was estimated using Lepto to evaluate the correction factors;
- the uncertainty due to the selection requirements was computed by varying the values of the cuts in data and MC. The largest effects were due to the cuts on jet transverse energy and hadronic angle.

All the above systematic uncertainties were added in quadrature. The absolute energy scale of the jets in data events was varied by its uncertainty of $\pm 3\%$ [37]. This uncertainty is highly correlated between measurements in different bins and is therefore treated separately. The uncertainty in the luminosity determination of 1.6% was not included.

7 QCD calculations

The differential jet cross sections presented in the next section are compared with the predictions of ARIADNE, LEPTO and fixed-order QCD calculations.

The ARIADNE MC model includes the CDM for parton showering, which mimics BFKL evolution. The LEPTO MC uses the DGLAP evolution. These models include approximations for higher-order effects in the QCD cascade. However, the model dependence of these approximations can be large. In fixed order QCD calculations, higher-order terms are treated analytically. However, uncertainties from missing higher-order corrections may be large.

The measurements were compared with QCD predictions evaluated using the event generator DISENT [38] which allows calculations that sum two orders of the perturbation series. The calculations were performed in the $\overline{\rm MS}$ renormalisation and factorisation schemes using a generalised version of the subtraction method [38]. The number of flavors was set to five; the renormalisation (μ_R) and factorisation (μ_F) scales were both set to $\mu_R = \mu_F = Q$; α_s was calculated at two loops using $\Lambda^{(5)}_{\overline{\rm MS}} = 220$ MeV, which corresponds to $\alpha_s(M_Z) = 0.1180$. The CTEQ6 [39] parameterisations of the proton PDFs were used. The results obtained with DISENT were cross-checked using the program DISASTER++ [40]; the differences were found to be less than 1% in most cases, and never exceeded 3%.

In the global phase space region, the sample is dominated by QPM type events. Therefore, the DISENT predictions in this region include the diagrams with $\mathcal{O}(\alpha_s^0)$ and $\mathcal{O}(\alpha_s^1)$. The BFKL and forward-BFKL phase-space regions are dominated by the contributions from BGF and QCDC processes and so the DISENT calculations include terms with $\mathcal{O}(\alpha_s^1)$ and $\mathcal{O}(\alpha_s^2)$.

The following sources of theoretical uncertainties were considered:

- the uncertainty in the calculations due to the absence of higher-order terms was estimated by varying μ_R by a factor of two. The effect on the calculation is between 5 and 50%, depending on the phase space region;
- the uncertainty in the calculations due to the uncertatinties in the proton PDF was estimated by repeating the calculations using 40 additional sets from CTEQ6. The resulting uncertainty was always below 5%.

8 Results

The measurements are presented as differential cross sections as functions of $\eta^{\rm jet}$, $E_T^{\rm jet}$, Q^2 and x_{Bj} in the three phase space regions. The cross sections as functions of $\eta^{\rm jet}$ and $E_T^{\rm jet}$ are measured including every jet in the event, whereas the cross sections as function of Q^2 and x_{Bj} are event cross sections for those events in the inclusive jet samples.

8.1 The global phase space region

The measurements are presented in Fig. 2. The cross section as a function of $\eta^{\rm jet}$ is suppressed in the forward region (high $\eta^{\rm jet}$) due to the lower cut on y. The measurements span $x_{\rm Bj}$ values between 0.0074 and .24.

The MC predictions and fixed-order QCD calculations are compared to the data in Fig. 2. The prediction of Ariadne describes all data distributions well, whereas the predictions from Lepto are slightly worse, especially at the lowest $x_{\rm Bj}$ values. The fixed order QCD calculations describe the data except at the high $\eta^{\rm jet}$ values and low $E_T^{\rm jet}$, Q^2 and $x_{\rm Bj}$ values. This excess of the data with respect to the calculations can be due to the absence of higher orders, since these calculations are only $\mathcal{O}(\alpha_s)$. The small uncertainty coming from the variation of μ_R might be underestimating the contribution from the higher orders, especially in these regions where the excess is largest. Alternatively, this excess might derive from the failure of the DGLAP evolution in this region of phase space, although LEPTO, which essentially includes higher order processes in a DGLAP ordering scheme, reproduces the data reasonably well.

8.2 The BFKL phase space region

The measurements are presented in Fig. 3. The shape of the cross section as a function of $\eta^{\rm jet}$ is steeply falling in the forward region due to the restriction on γ_h. The predictions of Ariadne describe all data distributions well. The predictions of Lepto fail to describe the data, especially the $\eta^{\rm jet}$ distribution and low $x_{\rm Bj}$ region. Fixed order QCD calculations, which are $\mathcal{O}(\alpha_s^2)$ in this phase-space region, describe the data well for Q^2, $E_T^{\rm jet}$ and $x_{\rm Bj}$, but understimate the data at high values of $\eta^{\rm jet}$. This disagreement is concentrated in a region where the cross section is small, and so it is not reflected in the other distributions. The uncertainty of the calculations due to the absence of higher orders is larger than before, but it is a more realistic estimation than in the global phase-space region. The uncertainty due to the parton shower model chosen has also increased. This is expected as the CDM mimics BFKL dynamics, whereas Lepto implements the same transverse energy ordering among the partons as in DGLAP. Disent can describe the data within the scale uncertainty over the entire Q^2, $E_{T,jet}$ and x_{Bj} regions, due to the fact that the discrepancy between data and DISENT in $\eta^{\rm jet}$ is limited to the forward region where the cross section is smallest.

8.3 The forward BFKL phase space region

The measurements are presented in Fig. 4. This phase space region is where events exhibiting BFKL effects are expected to be dominant. As expected, the predictions of ARIADNE describe the data well, whereas the predictions of LEPTO fail in all distributions. Fixed order QCD calculations are consistently lower than the data for $E_T^{\rm jet}$ and Q^2. The calculations describe the measurement as a function of $x_{\rm Bj}$ at high values, but underestimate the data in the low x_{Bj} region by nearly a factor of two. The uncertainty due to the missing higher orders is larger by nearly a factor of two than that in the BFKL phase-space region.

9 Summary and Conclusion

Measurements of differential cross sections in $E_T^{\rm jet}$, $\eta^{\rm jet}$, Q^2 and x_{Bj} for inclusive jet production in neutral current deep inelastic scattering have been presented using 38.7 pb^{-1} of ZEUS data. The low x_{Bj} region has been probed for events with $Q^2 > 25$ GeV^2 and at least one jet with 6 GeV of transverse energy. Three phase space regions have been studied: one inclusive region (global phase space), one with an additional requirement on the hadronic angle of the event ($\cos\gamma_h < 0$) and a more limited window of jet pseudorapidity ($\eta_{jet} > 0$), as well as the DGLAP suppression requirement $0.5 < \frac{E^2_{T,jet}}{Q^2} < 2.0$ (BFKL phase space), and finally the region with $2 < \eta^{\rm jet} < 3$ (forward BFKL phase space). The restrictions imposed in the BFKL phase space regions enhance the dijet and multijet contributions without restricting the transverse energy of the jet(s) at the top of the gluon ladder.

The leading-logarithm parton shower MC models can describe the shape of the data in most variables, but the Colour-Dipole Model generally gives a better description both in shape and normalization than the parton shower model MEPS.

A large excess of the data over the fixed-order QCD calculation is observed in the global phase-space region at high $\eta^{\rm jet}$ and low x_{Bj} , which are possibly the result of missing higher orders. This excess is significantly diminished in the BFKL phase space where the cross section is dominated by boson-gluon fusion events. However, the theoretical uncertainties increase significantly. In the BFKL phase-space region, the calculations give, in general, a good description of the data, although a slight excess of the data over the prediction is observed at high $\eta^{\rm jet}$. In the forward BFKL region, the shape of the measured $E_T^{\rm jet}$ and Q^2 cross sections are described, but fails to describe the shape in x_{Bj}. The uncertainty induced by the variation of the renormalization scale is large, indicating that missing higher order or $\ln(1/x)$ terms in the calculation could be important in this region. Accordingly, the present theoretical limitations prevent establishing an environment suitable for decisive tests of BFKL dynamics in these data. Improved calculations, perhaps using the BFKL approach, are needed to give a more accurate prediction in this region.

References

[1] V.N. Gribov and L.N. Lipatov, Sov. J. Nucl. Phys. **15**, 438 (1972);
L.N. Lipatov, Sov. J. Nucl. Phys. **20**, 94 (1975);
Yu.L. Dokshitzer, Sov. Phys. JETP **46**, 641 (1977);
G. Altarelli and G. Parisi, Nucl. Phys. **B 126**, 298 (1977).

[2] E.A. Kuraev, L.N. Lipatov and V.S. Fadin, Sov. Phys. JETP **45**, 199 (1977);
Ya.Ya. Balitskiĭ and L.N. Lipatov, Sov. J. Nucl. Phys. **28**, 822 (1978).

[3] M. Ciafaloni, Nucl. Phys. **B 296**, 49 (1988);
S. Catani, F. Fiorani and G. Marchesini, Phys. Lett. **B 234**, 339 (1990).

[4] ZEUS Coll., Preprint DESY-03-214, DESY, 2003. Subm. to Phys. Rev. D.

[5] ZEUS Coll., S. Chekanov et al., Phys. Lett. **B 547**, 164 (2002).

[6] ZEUS Coll., S. Chekanov et al., Phys. Rev. **D 67**, 012007 (2003).

[7] ZEUS Coll., J. Breitweg et al., Phys. Lett. **B 507**, 70 (2001).

[8] H1 Coll., C. Adloff et al., Eur. Phys. J. **C 30**, 1 (2003).

[9] H1 Coll., C. Adloff et al., Phys. Lett. **B 542**, 193 (2002).

[10] H1 Coll., C. Adloff et al., Phys. Lett. **B 515**, 17 (2001).

[11] A.H. Mueller, Nucl. Phys. Proc. Suppl. **C 18**, 125 (1991);
A.H. Mueller, J. Phys. **G 17**, 1443 (1991);
J. Bartels, A. De Roeck, M. Loewe, Z. Phys. **C 54**, 645 (1992);
J. Kwiecinski, A.D. Martin, P.J. Sutton, Phys. Lett. **B 287**, 254 (1992);
W.K. Tang, Phys. Lett. **B 278**, 363 (1992).

[12] ZEUS Coll., J. Breitweg et al., Eur. Phys. J. **C 6**, 239 (1999).

[13] ZEUS Coll., J. Breitweg et al., Phys. Lett. **B 474**, 223 (2000).

[14] H1 Coll., C. Adloff et al., Nucl. Phys. **B 538**, 3 (1999).

[15] H. Jung, Comp. Phys. Comm. **86**, 147 (1995).

[16] Y. Azimov et al., Phys. Lett. **B 165**, 147 (1985);
G. Gustafson, Phys. Lett. **B 175**, 453 (1986);
G. Gustafson and U. Pettersson, Nucl. Phys. **B 306**, 746 (1988);
B. Andersson et al., Z. Phys. **C 43**, 625 (1989).

[17] ZEUS Coll., M. Derrick et al., Phys. Lett. **B 293**, 465 (1992).

[18] ZEUS Coll., U. Holm (ed.), *The ZEUS Detector*. Status Report (unpublished), DESY (1993), available on `http://www-zeus.desy.de/bluebook/bluebook.html`.

[19] N. Harnew et al., Nucl. Inst. Meth. **A 279**, 290 (1989);
B. Foster et al., Nucl. Phys. Proc. Suppl. **B 32**, 181 (1993);
B. Foster et al., Nucl. Inst. Meth. **A 338**, 254 (1994).

[20] M. Derrick et al., Nucl. Inst. Meth. **A 309**, 77 (1991);
A. Andresen et al., Nucl. Inst. Meth. **A 309**, 101 (1991);
A. Caldwell et al., Nucl. Inst. Meth. **A 321**, 356 (1992);
A. Bernstein et al., Nucl. Inst. Meth. **A 336**, 23 (1993).

[21] J. Andruszków et al., Preprint DESY-92-066, DESY, 1992;
ZEUS Coll., M. Derrick et al., Z. Phys. **C 63**, 391 (1994);
J. Andruszków et al., Acta Phys. Pol. **B 32**, 2025 (2001).

[22] S.Catani et al., Nucl. Phys. **B406**, 187 (1993).

[23] S.D. Ellis and D.E. Soper, Phys. Rev. **D 48**, 3160 (1993).

[24] ZEUS Coll., S. Chekanov et al., Preprint hep-ex/0208037, 2002.

[25] F. Jacquet and A. Blondel, *Proceedings of the Study for an ep Facility for Europe*, 1979.

[26] S. Bentvelsen, J. Engelen and P. Kooijman, *Proc. Workshop on Physics at HERA*, W. Buchmüller and G. Ingelman (eds.), Vol. 1, p. 23. Hamburg, Germany, DESY (1992).

[27] J.E. Huth et al., *Research Directions for the Decade. Proceedings of Summer Study on High Energy Physics, 1990*, E.L. Berger (ed.), p. 134. World Scientific (1992). Also in preprint FERMILAB-CONF-90-249-E.

[28] R. Brun et al., GEANT3, Technical Report CERN-DD/EE/84-1, CERN, 1987.

[29] G. Ingelman, A. Edin and J. Rathsman, Comp. Phys. Comm. **101**, 108 (1997).

[30] A. Kwiatkowski, H. Spiesberger and H.-J. Möhring, Comp. Phys. Comm. **69**, 155 (1992). Also in *Proc. Workshop Physics at HERA*, 1991, DESY, Hamburg.

[31] K. Charchula, G.A. Schuler and H. Spiesberger, Comp. Phys. Comm. **81**, 381 (1994);
H. Spiesberger, HERACLES *and* DJANGOH*: Event Generation for ep Interactions at HERA Including Radiative Processes*, 1998, available on `http://www.desy.de/~hspiesb/djangoh.html`.

[32] L. Lönnblad, Comp. Phys. Comm. **71**, 15 (1992);
L. Lönnblad, Z. Phys. **C 65**, 285 (1995).

[33] ZEUS Coll., J. Breitweg et al., Eur. Phys. J. **C 11**, 251 (1999).

[34] B. Andersson et al., Phys. Rep. **97**, 31 (1983).

[35] T. Sjöstrand, Comp. Phys. Comm. **82**, 74 (1994).

[36] H.L. Lai et al., Phys. Rev. **D 55**, 1280 (1997).

[37] S. Lammers and D. Chapin, *Jet Energy Scale Uncertainty*, 2001. ZEUS Internal Note 01-006.

[38] S. Catani and M.H. Seymour, Nucl. Phys. **B 485**, 291 (1997). Erratum in Nucl. Phys. **B 510**, 503 (1998).

[39] J. Pumplin et al., JHEP **0207**, 012 (2002).

[40] D. Graudenz, Preprint hep-ph/9708362, 1997;
D. Graudenz, Preprint hep-ph/9710244, 1997.

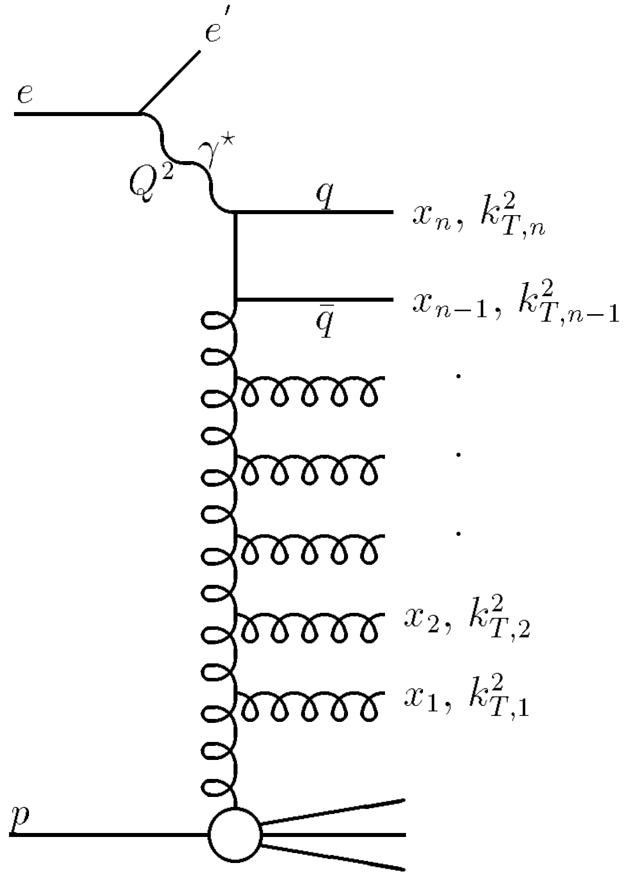

Figure 1: *Gluon ladder Feynman Diagram. In DGLAP, the final state partons are ordered in virtuality, with the highest virtuality on the photon side. This implies an ordering in transverse energy $k^2_{T,n} > k^2_{T,n-1} > k^2_{T,1}$. In BFKL, the partons do not have a strict k_T ordering.*

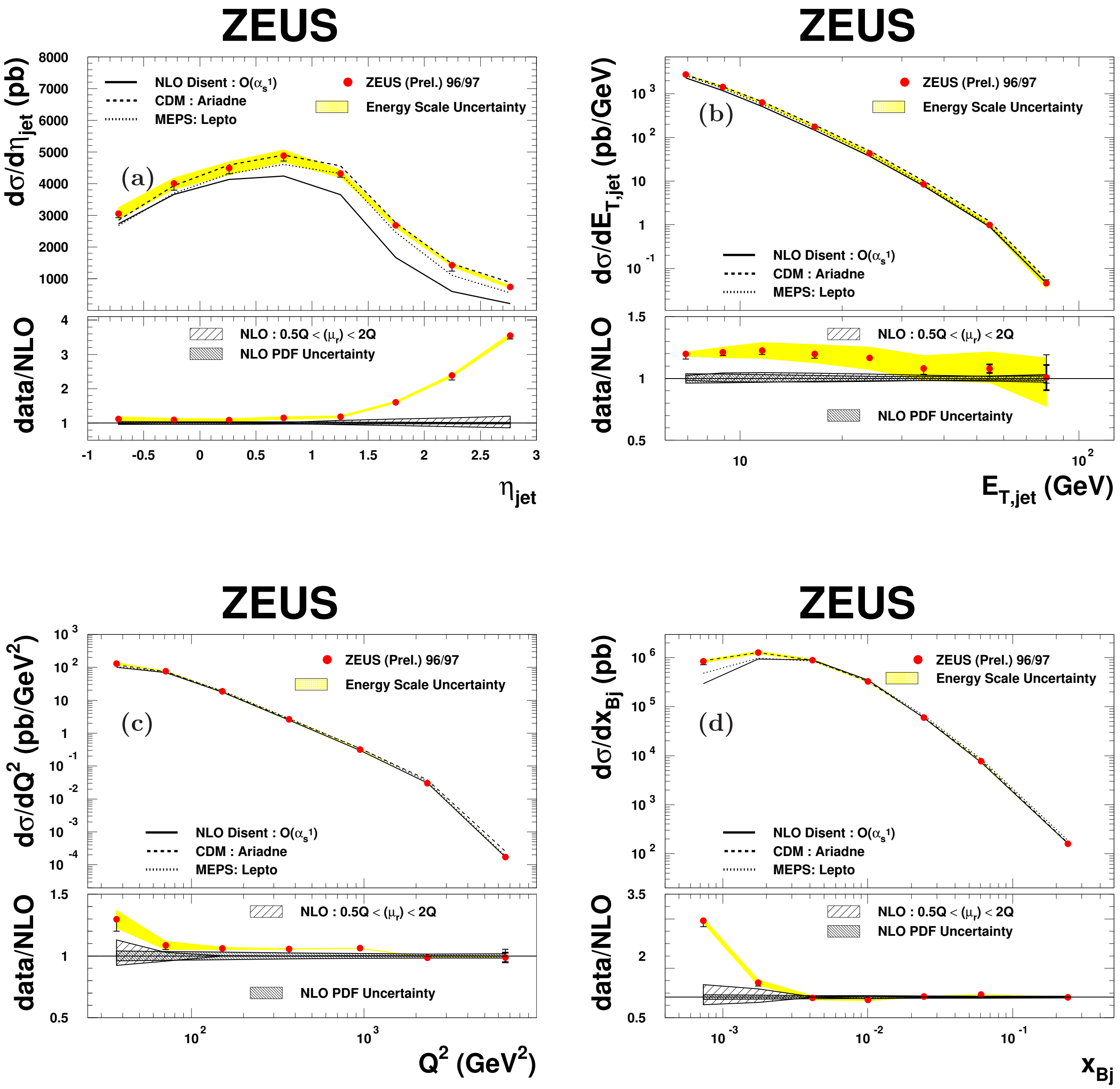

Figure 2: *Measured differential cross sections (dots) in the global phase space for inclusive jet production in NC DIS with $E_T^{\rm jet} > 6$ GeV and $-1 < \eta^{\rm jet} < 3$ in the kinematic region defined by $Q^2 > 25$ GeV^2 and $y > 0.04$ as functions of (a) $\eta^{\rm jet}$, (b) $E_T^{\rm jet}$, (c) Q^2 and (d) $x_{\rm Bj}$. The thick error bars represent the statistical uncertainty of the data (not visible), and the thin error bars show the systematic uncertainties not associated with the uncertainty in the absolute energy scale of the jets, which is shown separately as a shaded band. The calculations of CDM (dashed lines), MEPS (dotted lines) and $\mathcal{O}(\alpha_s)$ QCD calculations (solid lines) are included. The lower section of each plot shows the ratio of data to the QCD calculations, and the theoretical uncertainties.*

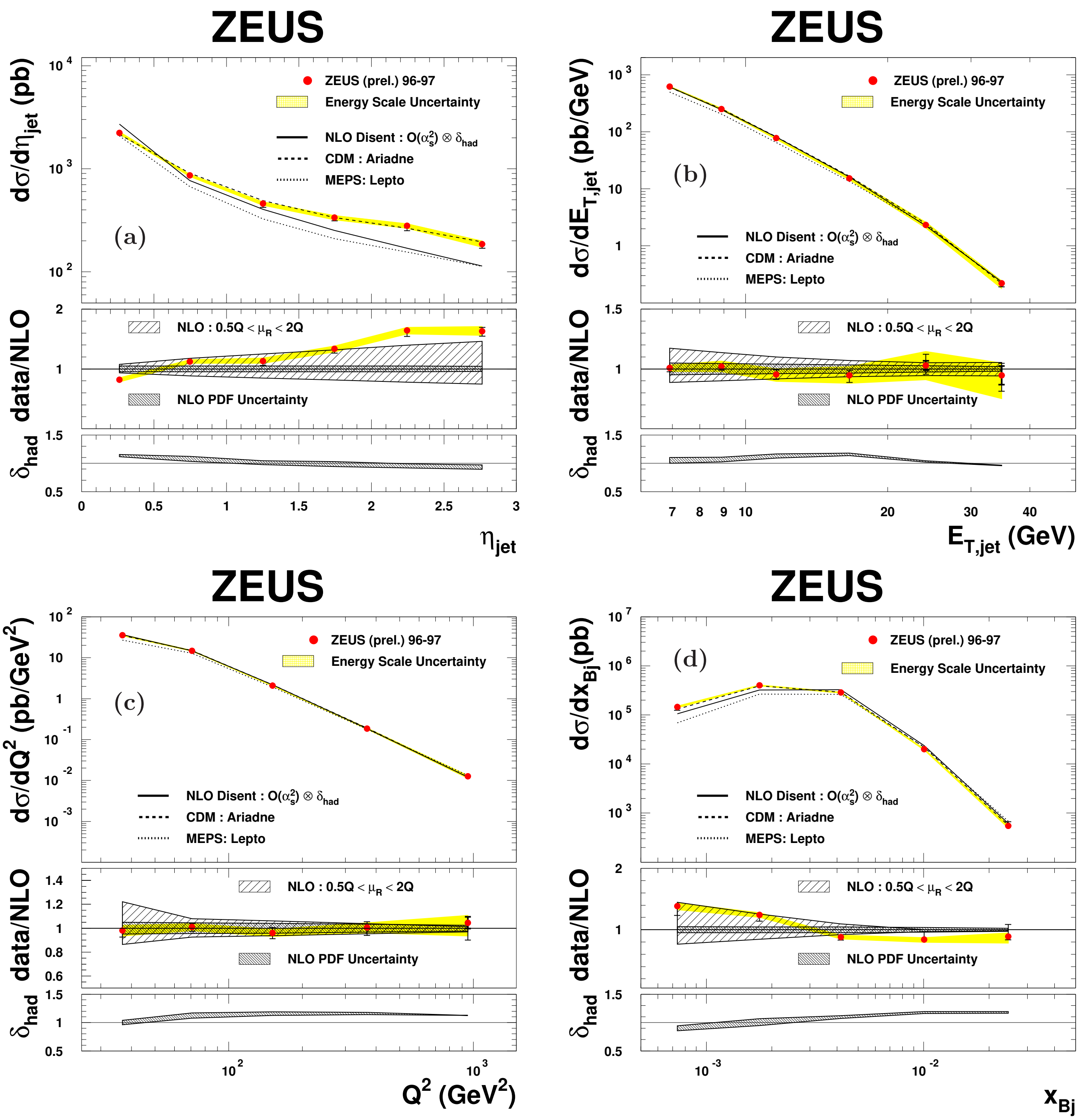

Figure 3: *Measured differential cross sections (dots) in the BFKL phase space for inclusive jet production in NC DIS with $E_T^{\rm jet} > 6$ GeV and $0 < \eta^{\rm jet} < 3$ in the kinematic region defined by $Q^2 > 25$ GeV^2, $y > 0.04$ and $\cos\gamma_h < 0$ as functions of (a) $\eta^{\rm jet}$, (b) $E_T^{\rm jet}$, (c) Q^2 and (d) $x_{\rm Bj}$. The lower section of each plot shows the hadronisation correction factor applied to the QCD calculations. Other details are as in the caption to Fig.2.*

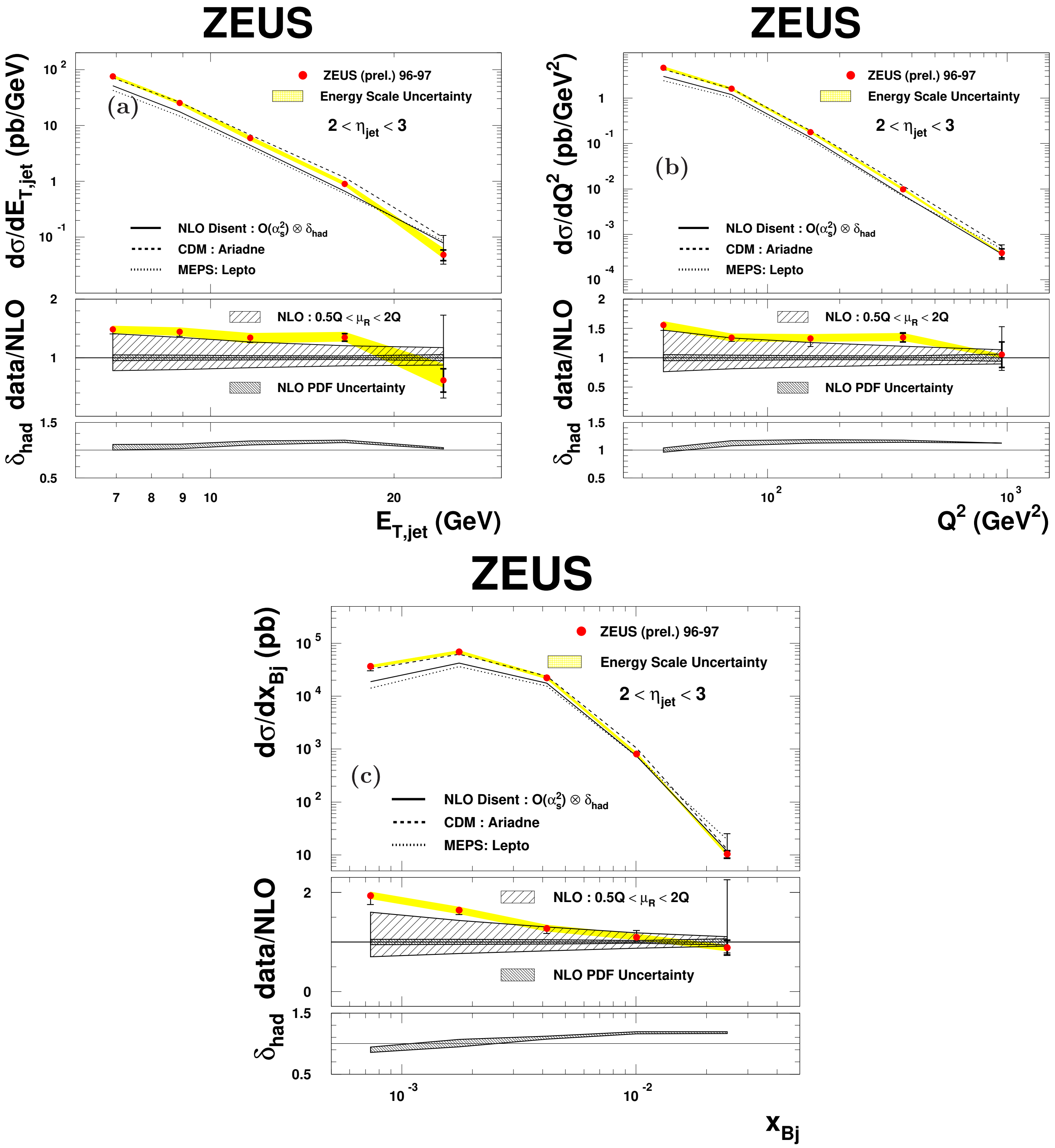

Figure 4: *Measured differential cross sections (dots) in the forward BFKL phase space for inclusive jet production in NC DIS with $E_T^{\rm jet} > 6$ GeV and $2 < \eta^{\rm jet} < 3$ in the kinematic region defined by $Q^2 > 25$ GeV^2, $y > 0.04$ and $\cos\gamma_h < 0$ as functions of (a) $E_T^{\rm jet}$, (b) Q^2 and (c) $x_{\rm Bj}$. The lower section of each plot shows the hadronisation correction factor applied to the QCD calculations. Other details are as in the caption to Fig.2.*